AD_____

GRANT NUMBER DAMD17-94-J-4292

TITLE: Improved Mammographic Technique for Breast Cancer

PRINCIPAL INVESTIGATOR: Heang-Ping Chan, Ph.D.

CONTRACTING ORGANIZATION: University of Michigan
Ann Arbor, Michigan 48109-1274

REPORT DATE: September 1997

TYPE OF REPORT: Annual

PREPARED FOR: Commander
U.S. Army Medical Research and Materiel Command
Fort Detrick, Frederick, Maryland 21702-5012

REPORT DOCUMENTATION PAGE

OMB No. 0704-0188

1. AGENCY USE ONLY *(Leave blank)*	2. REPORT DATE	3. REPORT TYPE AND DATES COVERED
	September 1997	Annual (11 Jul 96 - 10 Jul 97)

4. TITLE AND SUBTITLE
Improved Mammographic Technique for Breast Cancer Diagnosis

5. FUNDING NUMBERS
DAMD17-94-J-4292

6. AUTHOR(S)
Heang-Ping Chan, Ph.D.

7. PERFORMING ORGANIZATION NAME(S) AND ADDRESS(ES)
University of Michigan
Ann Arbor, Michigan 48109-1274

8. PERFORMING ORGANIZATION REPORT NUMBER

9. SPONSORING/MONITORING AGENCY NAME(S) AND ADDRESS(ES)
Commander
U.S. Army Medical Research and Materiel Command
Fort Detrick, Frederick, Maryland 21702-5012

10. SPONSORING/MONITORING AGENCY REPORT NUMBER

11. SUPPLEMENTARY NOTES

12a. DISTRIBUTION / AVAILABILITY STATEMENT
Approved for public release; distribution unlimited

12b. DISTRIBUTION CODE

13. ABSTRACT *(Maximum 200*

The goal of the proposed research is to improve the sensitivity of cancer detection in mixed or dense breasts through optimization of mammographic techniques. We propose to develop a novel exposure equalization system that preferentially reduces the incident x-ray intensity in the peripheral region of the breast, thereby alleviating the problem of limited latitude of x-ray detectors. Optimal imaging technique can then be developed for improving image quality throughout the entire breast.

We have performed the following studies in the third year of the funding period: (1) completed the study of breast shape classification, (2) conducted a simulation study to evaluate the effects of x-ray equalization, (3) completed the Monte Carlo modeling of a mammographic imaging system with a focused antiscatter grid, (4) constructed prototype filters and evaluated filter alignment by imaging breast phantoms, (5) conceived an improved method for implementation of the x-ray equalization technique for mammography, (6) conducted preliminary studies to demonstrate the feasibility of the new approach, and (7) developed design specifications for the compressible tank component of the patient-specific and tissue-equivalent x-ray equalization system. The development of the new method is a significant step towards the practical implementation of the x-ray equalization technique.

14. SUBJECT TERMS
Breast Cancer Mammography, exposure equalization, dynamic range compression, breast cancer detection

15. NUMBER OF PAGES
23

16. PRICE CODE

17. SECURITY CLASSIFICATION OF REPORT	18. SECURITY CLASSIFICATION OF THIS PAGE	19. SECURITY CLASSIFICATION OF ABSTRACT	20. LIMITATION OF ABSTRACT
Unclassified	Unclassified	Unclassified	Unlimited

FOREWORD

Opinions, interpretations, conclusions and recommendations are those of the author and are not necessarily endorsed by the U.S. Army.

____ Where copyrighted material is quoted, permission has been obtained to use such material.

____ Where material from documents designated for limited distribution is quoted, permission has been obtained to use the material.

HPC Citations of commercial organizations and trade names in this report do not constitute an official Department of Army endorsement or approval of the products or services of these organizations.

____ In conducting research using animals, the investigator(s) adhered to the "Guide for the Care and Use of Laboratory Animals," prepared by the Committee on Care and Use of Laboratory Animals of the Institute of Laboratory Resources, National Research Council (NIH Publication No. 86-23, Revised 1985).

HPC For the protection of human subjects, the investigator(s) adhered to policies of applicable Federal Law 45 CFR 46.

____ In conducting research utilizing recombinant DNA technology, the investigator(s) adhered to current guidelines promulgated by the National Institutes of Health.

____ In the conduct of research utilizing recombinant DNA, the investigator(s) adhered to the NIH Guidelines for Research Involving Recombinant DNA Molecules.

____ In the conduct of research involving hazardous organisms, the investigator(s) adhered to the CDC-NIH Guide for Biosafety in Microbiological and Biomedical Laboratories.

Chan Heang Ping 9/5/97

PI - Signature Date

(4) Table of Contents

(5) Introduction

Breast cancer is one of the leading causes of death among women. There is considerable evidence that early diagnosis and treatment significantly improve the chance of survival for patients with breast cancer (refs. 1-6). At present, x-ray mammography is the only diagnostic procedure with a proven capability for detecting early-stage, clinically occult breast cancers (refs. 5-8). Although mammography has a high sensitivity for detection of breast cancer when compared to other diagnostic procedures, studies indicate that radiologists identify only 70 to 90% of the lesions present (refs. 4-6, 9-11). The miss rate is particularly high in dense breasts (refs. 12, 13).

One of the difficulties in interpretation of mammograms by radiologists is caused by the limited latitude and contrast sensitivity of mammographic screen/film systems. Mammographic abnormalities related to early breast cancers include clustered microcalcifications, spiculated and irregular masses, areas of parenchymal distortion, and skin thickening (refs. 14, 15). These abnormalities are often subtle and low contrast. Therefore, low energy radiation and high contrast screen/film systems are recommended for mammographic imaging in order to increase the contrast between the lesion and the background tissue. Despite the use of vigorous compression during examinations (ref. 16), the low-energy x-ray beam results in a wide dynamic range (the ratio of the maximum to the minimum x-ray exposure at the detector) for the radiation penetrating the breast. This range can be greater than 100 (ref. 17) . On the other hand, high-contrast film provides a narrow latitude which is about 10 for a typical mammographic system (refs. 18, 19). As a result, thick and glandular regions of the breast are often imaged at the toe of the sigmoid-shaped sensitometric curve of the screen/film system; whereas, thin peripheral regions are imaged at the shoulder. The contrast and signal-to-noise ratio (SNR) of mammographic features are greatly reduced in these regions due to decreased film gradient and increased noise. The contrast sensitivity of the human visual system also drops rapidly as the film density increases (refs. 20-22). Kopans (ref. 12) found that 70% of breast cancers in women with dense breasts are in the periphery of the mammary parenchyma adjacent to the subcutaneous fat or retromammary fat. The poor image quality in the peripheral region thus imposes a serious limitation on the sensitivity of cancer detection in breasts with dense fibroglandular tissue.

We proposed a practical and cost-effective exposure equalization method for reducing the dynamic range of the x-ray image. The shapes of compressed breasts of the patient population will be analyzed and classified into a finite number of groups. A shaped filter for attenuating x-rays in the peripheral region of the breasts will be fabricated for each group. For a given patient, the breast shape during compression will be classified into one of these groups and the filter for the selected group will be used for this patient. With this technique, the dynamic range of the x-ray intensities incident on the recording system will be reduced and the entire image can be recorded in the high contrast region of the film. The improved image quality can be achieved without additional radiation dose to the patient. Furthermore, a very high-contrast mammographic technique may be developed in combination with exposure equalization to further improve the signal-to-noise ratio (SNR) of the subtle lesions. We expect that the optimized technique will significantly improve the detectability of cancers in mixed and dense breasts and increase the efficacy of mammography as a screening and diagnostic tool for breast cancers.

In the course of the research, we have conceived a new approach to the implementation of an x-ray equalization filter for mammography. In this new approach, the patient breast will be immersed in a compressible tank containing a tissue-equivalent fluid which is compressed together with the breast for the x-ray exposure. The fluid will fill any space between the breast, the cassette holder and the compression paddle. Therefore, the filter is truly patient specific and tissue-equivalent. We have performed preliminary studies to identify possible tissue-equivalent liquids and to design the compressible tank. Detailed discussion is included in the Body of this report.

(6) Body

In the second year (7/11/96-7/10/97) of this grant, we have performed the following studies:

(a) Completion of the study of breast shape classification

We reported the results of our study of breast shape classification for designing filters in last year's progress report. An issue that was not addressed in last year's study is how to establish a more objective way to determine the optimum number of breast shape filters. In general, better fits between the filters and the individual breast borders within each class are achieved when more classes and therefore greater numbers of filters are employed. However, use of a large number of filters would make implementation of our equalization technique impractical and expensive. To assess the effect of using different numbers of filters, we previously used the average RMS distances between the breast borders in a given group and the average filter for that group as a measure of the "goodness of the filter". The average RMS distances were computed for a variety of classification schemes in which 2 to 10 classes (and filters) were employed. Recently, we developed two statistics to better evaluate the goodness of the classification and compared the relative merits of classification into different number of classes.

One of the new statistics that we derived to assess the goodness of a filtration scheme is the overall mean RMS distance for all of the filters within that scheme. It was computed using the equation:

$$\bar{d} = \frac{\sum_{g=1}^{N} \sum_{i=1}^{P_g} RMS_i}{T},$$

where N is the total number of clusters (e.g., 2, 3, 4, 5, 6, 8 or 10), P_g is the number of borders in cluster g, RMS_i is the RMS distance between border i and the filter for cluster g, and T is the total number of borders (e.g., $T = \sum_{g=1}^{N} P_g$).

The second statistic is a figure of merit (FOM). The equation employed was:

$$FOM = \frac{\sum_{g=1}^{N} \left(P_g / (\overline{RMS_g})^2\right)}{\sqrt{N}},$$

where P_g and N are as defined above, and $\overline{RMS_g}$ is the average RMS error for cluster g. The denominator in this equation ($\sqrt{N}$) is a term that penalizes the use of larger numbers of clusters, and the numerator gives greater weight to those clusters having greater number of borders and smaller RMS errors.

The overall mean RMS errors are listed in Table 1, below, and the FOM is plotted in Figure 1. The results in Table 1 indicate that the goodness-of-fit, as represented by the overall mean RMS distance error, generally improves as the number of clusters increases. However, the improvement is not very great beyond 3 or 4 clusters. This is true for both the CC-view and MLO-view data as well as for the filters formed by fitting the original compressed breast borders

with two coefficient (a,b), and 3-coefficient (a,b,c) polynomials. The figures of merit shown in Figure 1 exhibit maximum values at 3 clusters. Taking both of these statistics into account, it appears that 3 or 4 filter shapes for each view are optimum. This estimate, however, ignores the differences in the exposure distribution striking the detector resulting from variations in the thicknesses of the breasts within each subclass. It is likely that three filters will be required to compensate for this effect for each breast shape class. For example one could employ filters offering different degrees of equalization for thick, medium, and thin breasts. Thus, the total number of filters required for each view will be around 9 or 12. Both of these numbers are within a practical range for the implementation of the equalization technique.

Table 1. Overall mean RMS distance between individual borders and "filters"

Overall Mean RMS Error (mm)

Total no. of clusters	CC-View ab-fit*	CC-View abc-fit**	MLO-View ab-fit*	MLO-View abc-fit**
2	3.02	3.11	2.54	3.34
3	2.73	3.05	2.33	3.18
4	2.68	2.97	2.25	3.24
5	2.67	2.98	2.19	3.11
6	2.66	2.97	2.18	3.12
8	2.48	2.91	2.12	3.07
10	2.48	2.89	2.09	3.11
6 hybrid	-	2.69	-	2.68
6 using Z-scores	-	2.99	-	-
6 (2 best from 6 clusters + re-cluster remaining into 4 clusters)	2.63	-	-	-
7 (2 best from 6 clusters + re-cluster remaining into 5 clusters)	2.63	-	-	-
8 (2 best from 6 clusters + re-cluster remaining into 6 clusters)	2.62	-	-	-
8 hybrid	-	3.03	-	-

*ab-fit = original compressed breast borders fit using the equation $y = ax^2 + bx^3$

**abc-fit = original compressed breast borders fit using the equation $y = ax^2 + bx^3 + cx^4$.

We have written a manuscript to summarize the classification study. It was submitted to the Medical Physics journal for consideration of publication in May of this year.

The significance of this study is that, using a large data base of about 500 mammograms in each mammographic view, the results support our hypothesis that a small number of pre-fabricated filters will be sufficient to allow selection of a nearly patient-specific filter for each breast being examined. This is the basis of our approach to exposure equalization in mammographic imaging.

(b) Simulation Study of Effects of Filter Alignment

We have conducted a simulation study to evaluate the effects of filter alignment on a filtered image. A ray tracing method is used to determine the change in the optical density at a given pixel location on a mammogram when a filter is inserted between the breast and the x-ray focal spot. A flow diagram of the steps of the simulation study in which a filtered mammogram is digitally derived from an unfiltered mammogram is shown in Fig. 2.

(1) A clinical mammogram is digitized. The optical density (OD) at a given location is represented by pixel values, as determined by the digitizer's calibration curve (a low OD is digitized to a large pixel value).

(2) The computer performs edge detection and determines the breast shape. Automatic classification is performed and a prefabricated filter that matches the shape of this breast is found.

(3) The pixel value of the digitized mammogram is converted to OD using the digitizer's calibration curve.

(4) The OD at a given pixel is converted to the relative incident exposure (E_t) to the film by using the sensitometric (H & D) curve.

(5) The primary exposure (E_p) to the film is derived from E_t by correcting for the scattered radiation (E_s) at the pixel location: $E_p = E_t [1 - E_s/(E_p + E_s)]$.

(6) The selected filter is automatically aligned to the breast. By tracing an x ray through the filter, the exposure reduction factor at a given pixel due to filter attenuation is determined.

(7) The primary exposure to the film after filtration is calculated and the total exposure, i.e., primary plus scatter, is derived by using the scatter fraction.

(8) The exposure is converted to OD by using the sensitometric curve of the film.

(9) The decrement in OD at the pixel location is calculated as the difference between the original unfiltered OD and the OD after filtration, and the corresponding increment in pixel value is looked up from the digitizer's calibration curve.

(10) The pixel value increment matrix is smoothed before being applied to the unfiltered mammogram to reduce the fluctuation created by the digital simulation process.

(11) The filtered image is derived by summing the unfiltered image with the smoothed pixel value increment matrix.

An example of a mammogram being filtered by the simulation process is shown in Fig. 3. Fig. 3(a) is the original unfiltered image. Fig. 3(b) is the pixel-dependent exposurereduction factors calculated from the selected filter for this breast. Fig. 3(c) is the filtered mammogram. It can be seen that the gray levels within the breast remains the same after filtration. Around the breast periphery, however, the OD is decreased and the visibility in this region is improved. In the nipple region, there is a slight shadowing because the nipple of this breast retracts and the filter shape and slope derived from an average breast cannot match this specific condition.

Notice that there are many artifacts outside the breast. They are caused by the digitizer and will not exist in a real filtering process. The horizontal streaks are caused by blooming and charge transfer of the CCD. The different intensities of the left and right sides of the image are due to the unbalanced sensitivities of two butted CCD sensors. These artifacts are strongly enhanced by the large uncertainties during sensitometric conversion from OD to relative exposure and vice versa in the extreme OD region outside the breast (shoulder of the H & D curve).

A second example demonstrating the effects of exposure equalization on a mammogram is shown in Fig. 4. The visibility of the periphery of the breast is again improved. The skin thickening near the nipple can be seen more clearly in the filtered image. The skin thickening is much denser than the normal skin lines. Some shadowing can be observed in the upper part of the breast boundary. This is probably caused by a mismatch between the 3-D profiles of the breast and the average filter.

The simulation studies indicate that, with automated breast shape classification, filter selection, and alignment, it is feasible to implement the external x-ray beam equalization technique in a mammography system. Furthermore, this implementation should only require minimal additional operator intervention. A filter designed for a given breast shape class can match fairly well to patient breasts in that class. Some mismatch artifacts can be observed locally, but they do not disturb the visibility of the structures in the breast image. For a given breast shape class, if additional filters of different thicknesses are built, e.g., three thicknesses for thick, medium, and thin breasts, respectively, matching of OD at the periphery will be improved. We are in the process of designing a figure-of-merit to quantify the degree of misalignment.

(c) Monte Carlo Modeling of Mammographic Imaging System

We have been developing a Monte Carlo simulation model of the mammographic imaging system (Fig. 5) using the MCNP code from the Los Alamos National Lab. In the progress report last year, we reported the simulation of photon scattering in mammographic imaging without an antiscatter grid. In the current year, we have completed modeling of the grid and have performed simulation studies to determine the distribution of scattered radiation recorded at the detector. Fig. 6. shows the comparison of the scatter fractions along a radius of our CIRS breast phantom as determined by Monte Carlo simulation and by experimental measurements for the case without grid and for the case with a grid. To evaluate the increase in the scatter fractions at the boundary of the breast, we simulated photon scattering in a flat slab of 50% glandular/50% fat material that did not have the elliptical cross section at the boundary. The comparison of the scatter fractions for the breast phantom and for the flat slab is shown in Fig. 7. It can be seen that the peak of the scatter fraction at the breast boundary was due mostly to the decrease in thickness towards the breast periphery. Both the primary and scattered radiation increased as the breast thickness decreased. However, the scattered radiation increased more rapidly than the primary radiation at the beginning, but the scatter eventually decreased when the breast thickness further decreased to near zero at the boundary. With exposure equalization, the peaking of the scatter fraction will not occur and the image contrast will be improved.

With the Monte Carlo simulation model, we plan to evaluate the dependence of image quality on the various imaging parameters, including the x-ray spectra from different anode materials, the kVp, screen-film and digital detectors, and antiscatter technique with an air gap or with a grid. The dependence of image quality on imaging technique will be studied for different breast composition and thicknesses, and with and without x-ray equalization. The technique parameters can then be optimized for each type of breast. The improvement of image quality with x-ray equalization will be determined.

(d) Prototype Filter Construction and Experimental Evaluation of Filter Alignment

After the classification of breast shapes, we could design an average filter for each of the breast shape groups. In last year's progress report, we discussed the determination of the exposures to the screen/film detector along normals to the filter border. The relative exposures along the normals were obtained for each breast border in a particular group. The average exposures along each normal for the breast shape group were then derived. An example of the average filter border for a given breast shape group and the normals to the breast border is shown in Fig. 8. With the average exposures along the normals to the breast borders for a given x-ray spectrum, we could calculate the filter thickness profiles along the normals. The filter thickness at a given point using a chosen material was equal to the thickness needed to attenuate the x-ray beam so that its intensity at the detector was about the same as the average intensity behind the central part of the breast. The thickness profiles along the discrete normals were then used to create a three-dimensional (3D) model of a solid filter by interpolating along the surface.

We evaluated two approaches for constructing an x-ray equalizing filter. These involve using either solid or liquid materials for the filter. If a solid material is used, the 3D model itself will be employed to fabricate the filter . If a liquid material is used, the 3D model will be employed to fabricate a negative mold for the filter. The two approaches are illustrated in Fig. 9. We had fabricated solid filters with aluminum and Teflon. We also constructed two thin negative molds to test the use of an iodine contrast agent as a filter material, as well as several negative molds with Styrofoam to test other liquid materials including barium sulfate, water, and saline. We compared breast phantom images taken with and without the x-ray equalizing filter using a GE DMR mammography system. A pair of unfiltered and filtered images of our 4.5-cm-thick CIRS breast phantom with 50% glandular/50% fat composition are shown in Fig. 10. The filter used in this example was a negative Styrofoam mold with saline as the filter material. It can be seen that the filter under-compensated the phantom periphery, probably because the slope and the curvature of the hand-crafted foam mold did not exactly match the border of the phantom. However, the visibility of the periphery region of the phantom image was improved after equalization, especially at the nipple region, where the fat envelope enclosing the phantom was clearly seen.

(e) New Approach to the Development of a Patient-Specific Filter

The experiments in x-ray equalization filter construction indicated that our new negative-mold method would be a more practical way to make an external equalization filter. Liquid or even solid filters can be made from a negative mold which is easier to fabricate than a solid machined filter. However, our experiments also revealed that the alignment of the equalization filter to the breast phantom is critical, even at a relatively large magnification factor. The projection of the filter edge to the phantom image is sharp so that misalignment will create clearly visible transition regions on the image. A computerized automatic alignment device will alleviate this problem, although some shadowing may still be observed in local regions on some breast images because of the slope and curvature mismatch, as demonstrated in the simulation study.

We have recently conceived a new technique that promises to be practical and will produce superior images. It will provide a truly patient-specific, tissue-equivalent filter around the patient's breast to reduce the x-ray intensity. Our new approach is to immerse the breast in a compressible tank containing a tissue-equivalent liquid, which will be compressed together with the breast for the x-ray exposure. The tissue-equivalent filter will therefore fit breasts of any thickness and shape, and it can be utilized to image the breast in any mammographic view. In order to avoid liquid leakage at the chest wall, the breast will be imaged in a new geometry similar to that employed in prone breast biopsy systems such that the compressible tank will be installed under the table. This approach will also allow combined mammography and ultrasound imaging in the future, which will further improve cancer detection. A commercially available Fischer biopsy table with an undertable x-ray tube and a conventional screen-film detector will be well-suited for this implementation of our new x-ray equalization technique. We are preparing a request for change in equipment purchase from the approved upright mammography system to this prone system. The request will be submitted separately.

We conducted a preliminary study to evaluate the effectiveness of this system. The preliminary study was performed with an upright mammography system. A CIRS breast phantom that has the shape of a compressed breast was placed horizontally in a rectangular container which contained a fluid filled up to the surface of the phantom. The fluid therefore filled all the space around the breast, simulating the situation with a compressible tank. We tested several fluids for their tissue equivalency including water, saline, mixtures of alcohol and water in different proportions, and emulsions with different fat contents ranging from 10% to 50%. Two different CIRS phantoms, one 4.5 cm thick with 50% glandular/50% fat composition, the other 6 cm thick with 20% glandular/80% fat composition, were tested with these potential filter materials. We

found that a 90% alcohol/10% water solution and an emulsion with 50% fat content were the best tissue-equivalent materials of those tested. Fig. 11 shows a comparison of the phantom images acquired before and after exposure equalization using the alcohol/water solution. Fig. 12 shows another example using the 50% fat emulsion. It can be seen that the periphery of the breast phantom images were almost perfectly equalized. Fig. 13 compares the optical density profiles along the radii at the periphery of the phantom images in Fig 11 before and after equalization. The optical densities after equalization were almost flat except for the narrow region across the fat envelope of the phantom. There were no misalignment artifacts caused by the filter, but there were some artifacts caused by air bubbles that formed around the phantom surfaces. These preliminary results indicate that the new approach for x-ray equalization is superior to the previously proposed method.

With this new approach, the major task is to design and construct the breast immersion/compression system. We have begun an initial design and set the following criteria in order that the system can be used practically for breast imaging:

(1) It should be a self-supporting structure, which is leakproof, durable, and flexible, permitting contraction and expansion in one dimension by about 10 cm.
(2) The system must contain a paddle section that can stand up to 40 lb. pressure and is used to compress the breast to a uniform thickness for x-ray mammography. It should consist of a material that has low x-ray attenuation properties.
(3) It should incorporate a sterile fluid handling subsystem for filling and emptying the tank with tissue-equivalent fluid and cleaning chemicals (This fluid handling subsystem should be designed to minimize air bubble formation since air bubbles cause artifacts in x-ray images).
(4) It should incorporate a drainage subsystem to prevent overflow of liquids, which will otherwise occur when the tank and the breast are compressed together for x-ray imaging.

(f) Miscellaneous

We had moved into the Cancer Geriatric Center (CGC) at the University of Michigan Hospital and set up an x-ray lab for mammographic imaging. The x-ray lab is adjacent to the Breast Imaging Division of the Radiology Department so that we have easy access to the film processors which are maintained under an MQSA approved quality assurance program. All of our experimental studies to date (filter design, test of tissue-equivalent materials, and phantom image comparisons) have been performed using one of the three state-of-the-art GE DMR mammography systems in the clinical area. Since these units are used routinely in the clinic, they may not be modified to incorporate significant changes for implementing our x-ray exposure equalization methods. Furthermore, the GE DMR systems are upright and therefore can not be utilized to implement our new technique. To develop that technique, we will purchase a used Fischer prone mammography system and install it in our lab as soon as our request for change of equipment purchase is approved.

(g) **Illustrations**

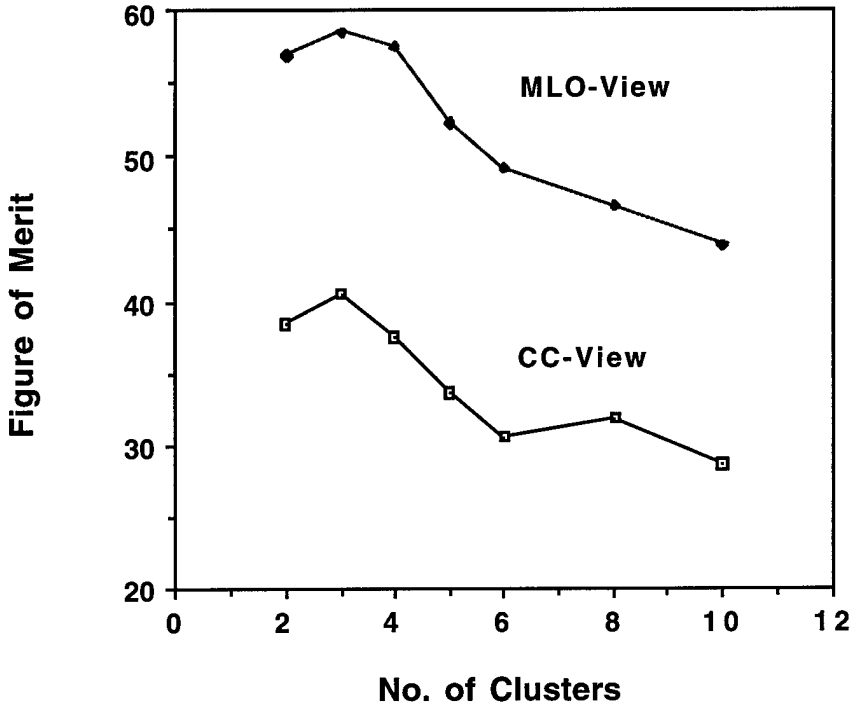

Fig. 1. Plots of clustering figure of merit as a function of the number of clusters for the CC and MLO-views. The two coefficient (a,b) fit data were employed in deriving the figure of merit.

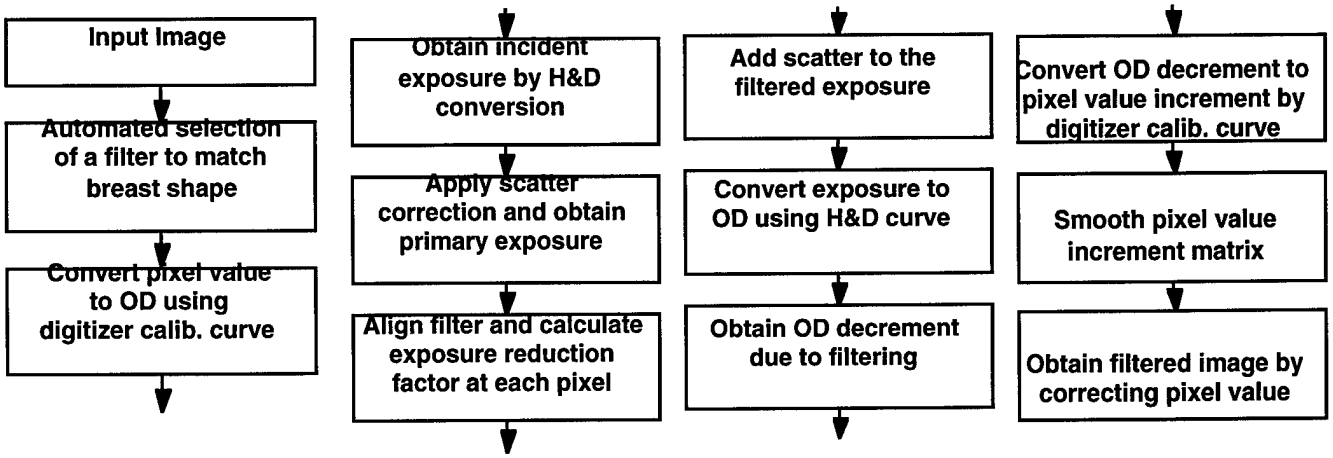

Fig. 2. Flow diagram of the simulation study for evaluation of the effects of x-ray equalization on mammograms.

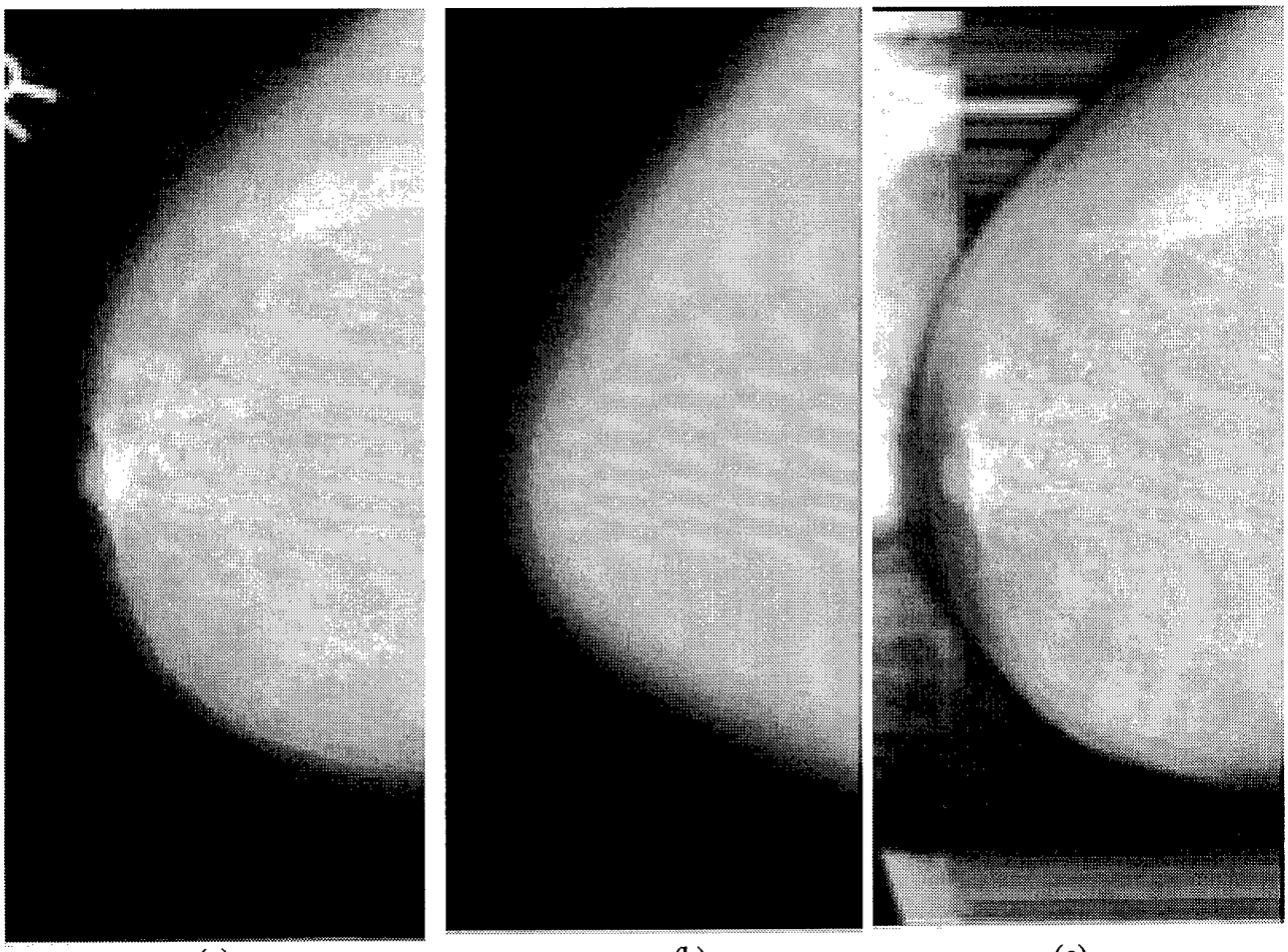

(a) (b) (c)

Fig. 3. An example of the simulation study. (a) an unfiltered mammogram, (b) the distribution of exposure reduction factor (illustrated as an image) due to insertion of the external beam filter, (c) the filtered mammogram.

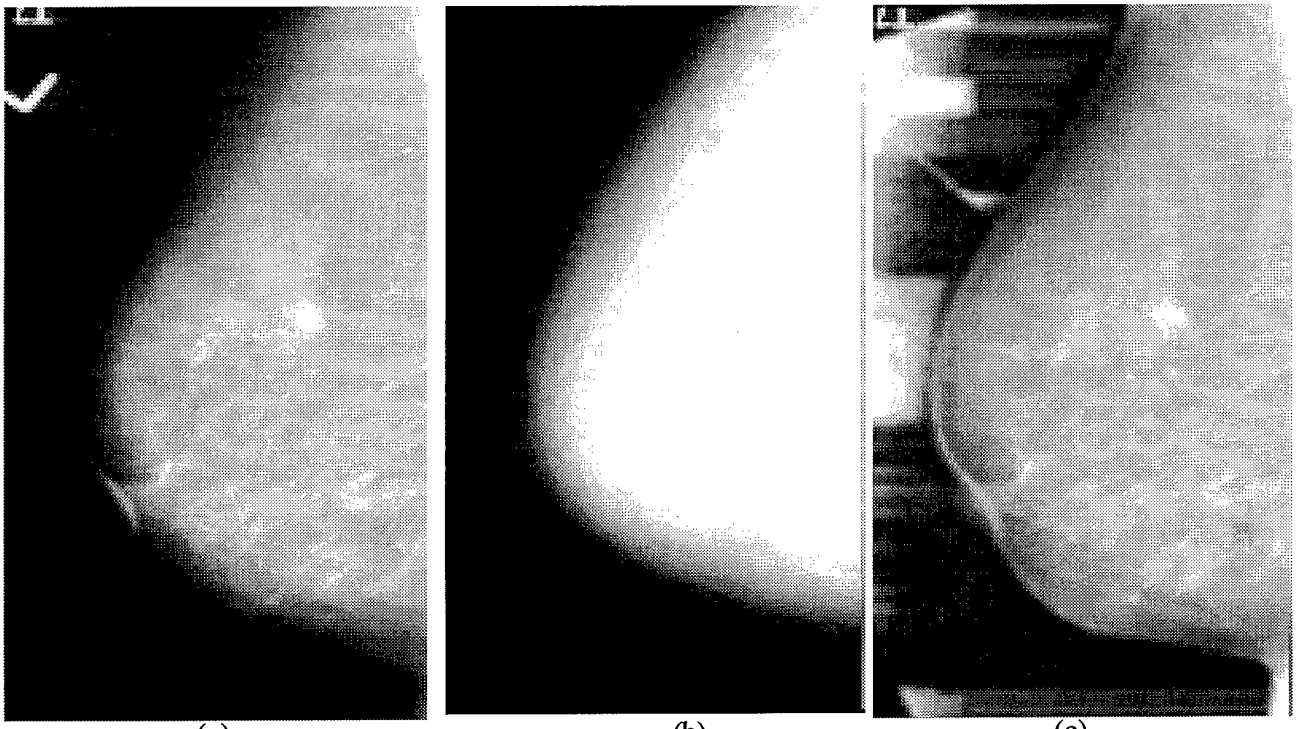

(a) (b) (c)

Fig. 4. A second example of the simulation study. (a) an unfiltered mammogram, (b) the distribution of exposure reduction factor (illustrated as an image) due to insertion of the external beam filter, (c) the filtered mammogram.

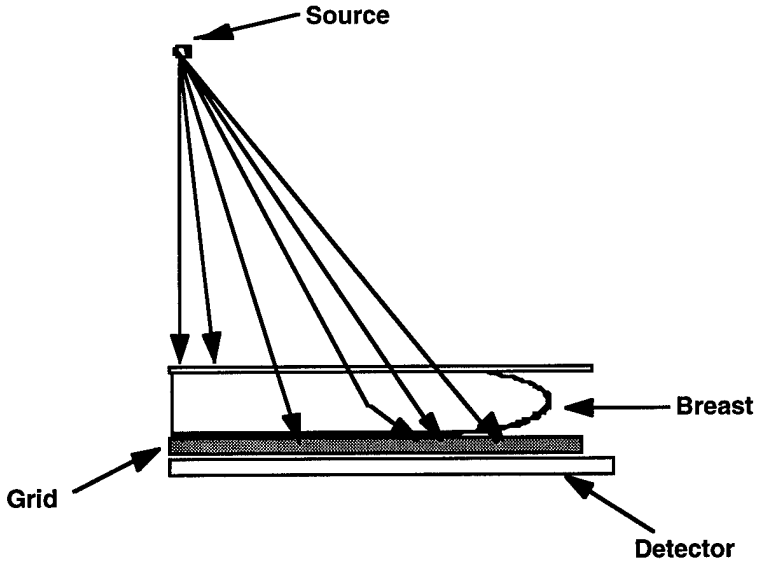

Fig. 5. Schematic of a mammographic imaging system modeled by Monte Carlo simulation.

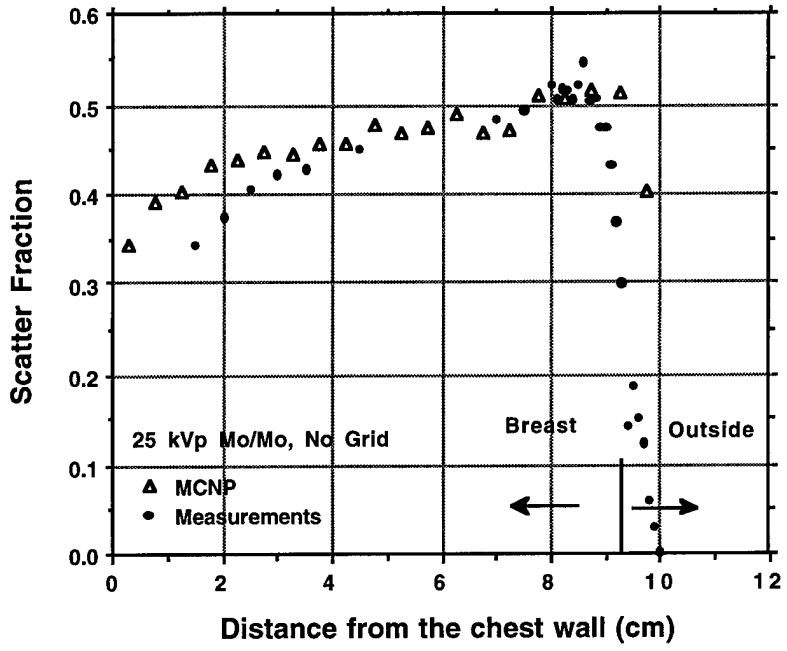

(a)

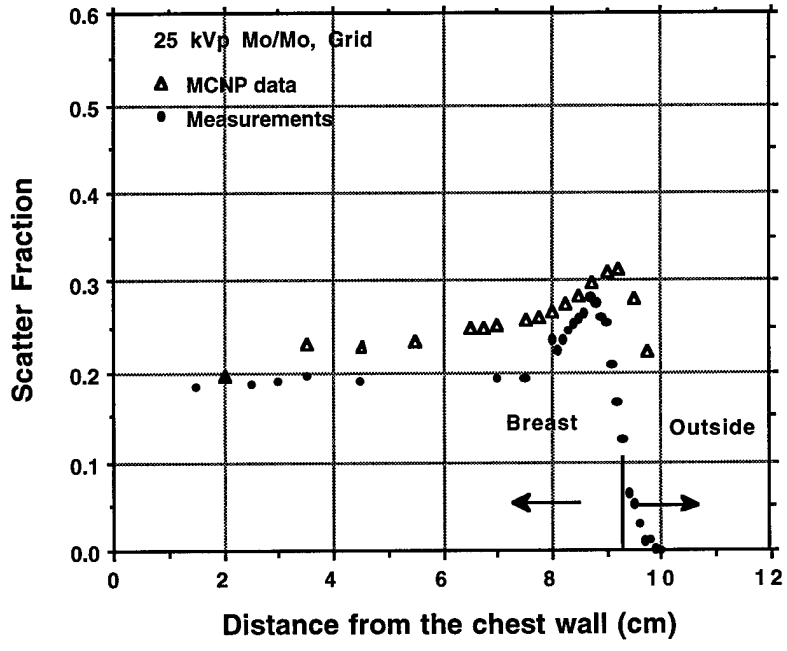

(b)

Fig. 6. Distribution of scatter fraction along a radius of the CIRS breast phantom: 3.7 cm 50% glandular/50% fat and 0.8 cm fat. (a) no grid, (b) with a 5:1 ratio, 31 lines/cm grid.

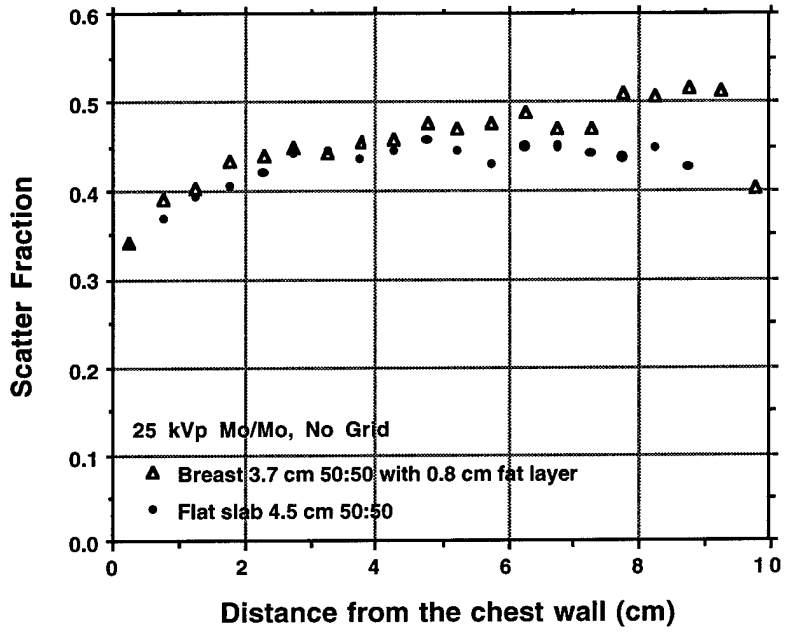

(a)

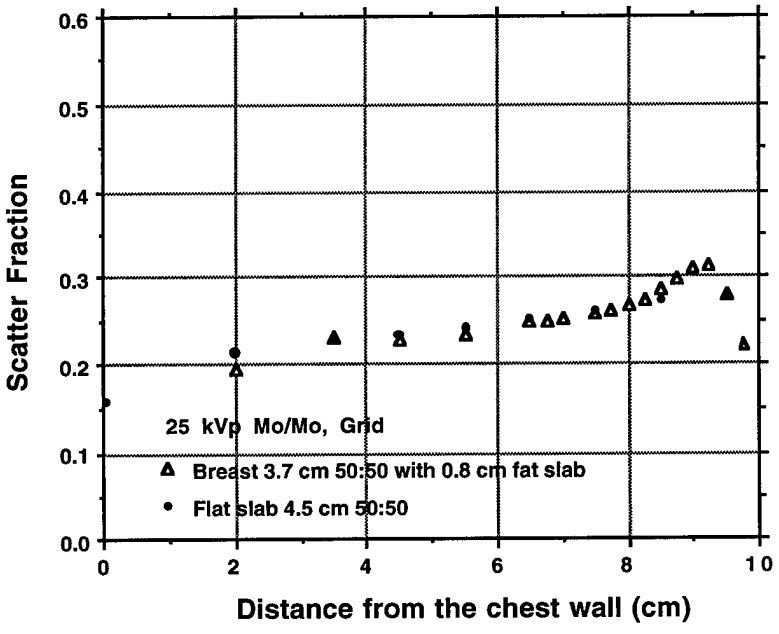

(b)

Fig. 7. Comparison of scatter fraction along a radius of our CIRS breast phantom (3.7 cm 50% glandular/50% fat and 0.8 cm fat) with that of a flat slab of 50% glandular/50% fat material. (a) no grid, (b) with a 5:1 ratio, 31 lines/cm grid.

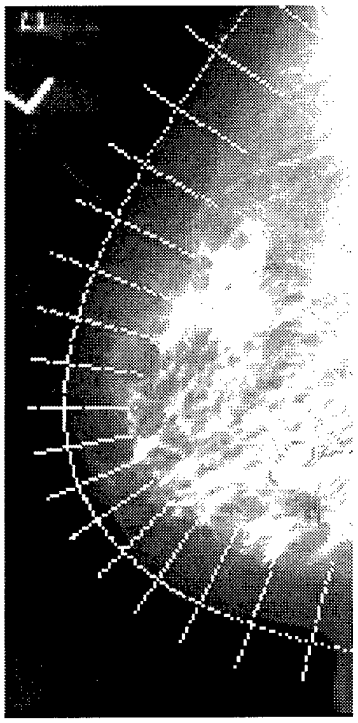

Fig. 8. Illustration of the normals to the average breast border (filter border) to be used for determination of the average exposure profiles at the breast periphery in the breast shape group. The normals were superimposed on one of the breast images in the group which was histogram equalized to better visualize the border location.

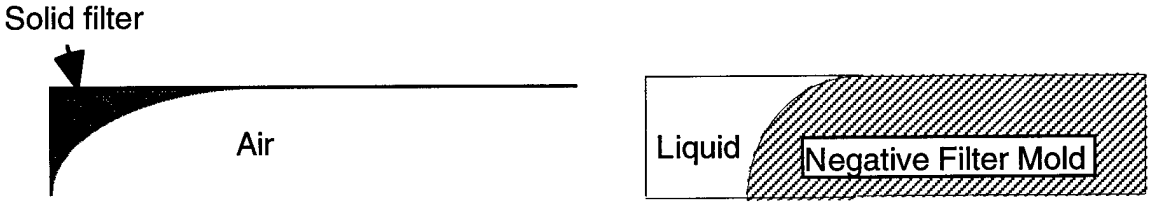

(a) (b)

Fig. 9. Two approaches for constructing an x-ray equalization filter. (a) solid filter, and (b) liquid filter.

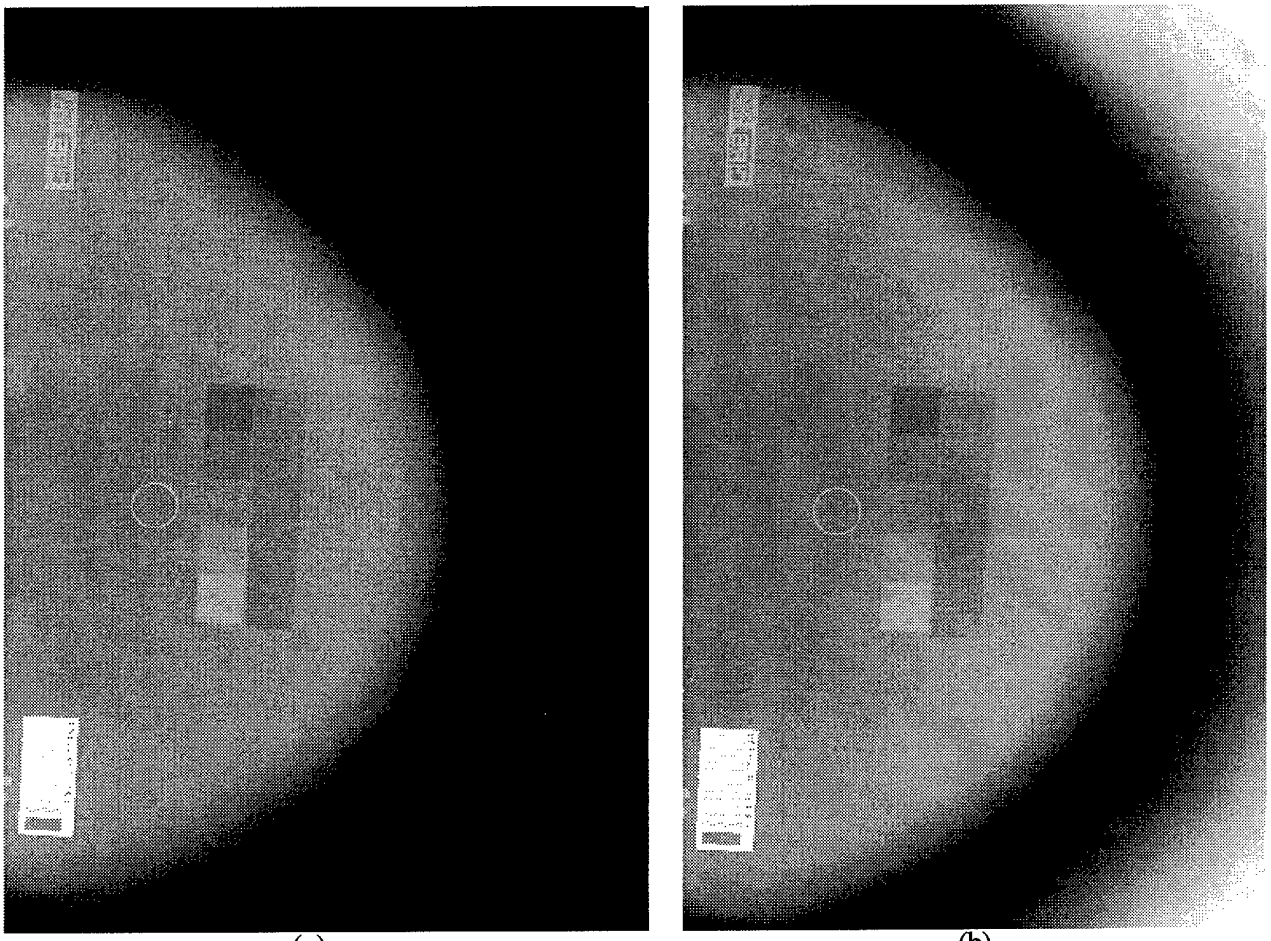

(a) (b)

Fig. 10. Comparison of (a) unequalized image and (b) equalized image of a CIRS phantom (4.5 cm thick 50% glandular/50% fat) exposed with a Mo/Mo 26 kVp beam. The filter was made of a breast shaped negative filter mold in a container, and the container was filled with saline. The border of the filter mold was aligned with the border of the phantom. The visibility of the phantom border was improved after equalization.

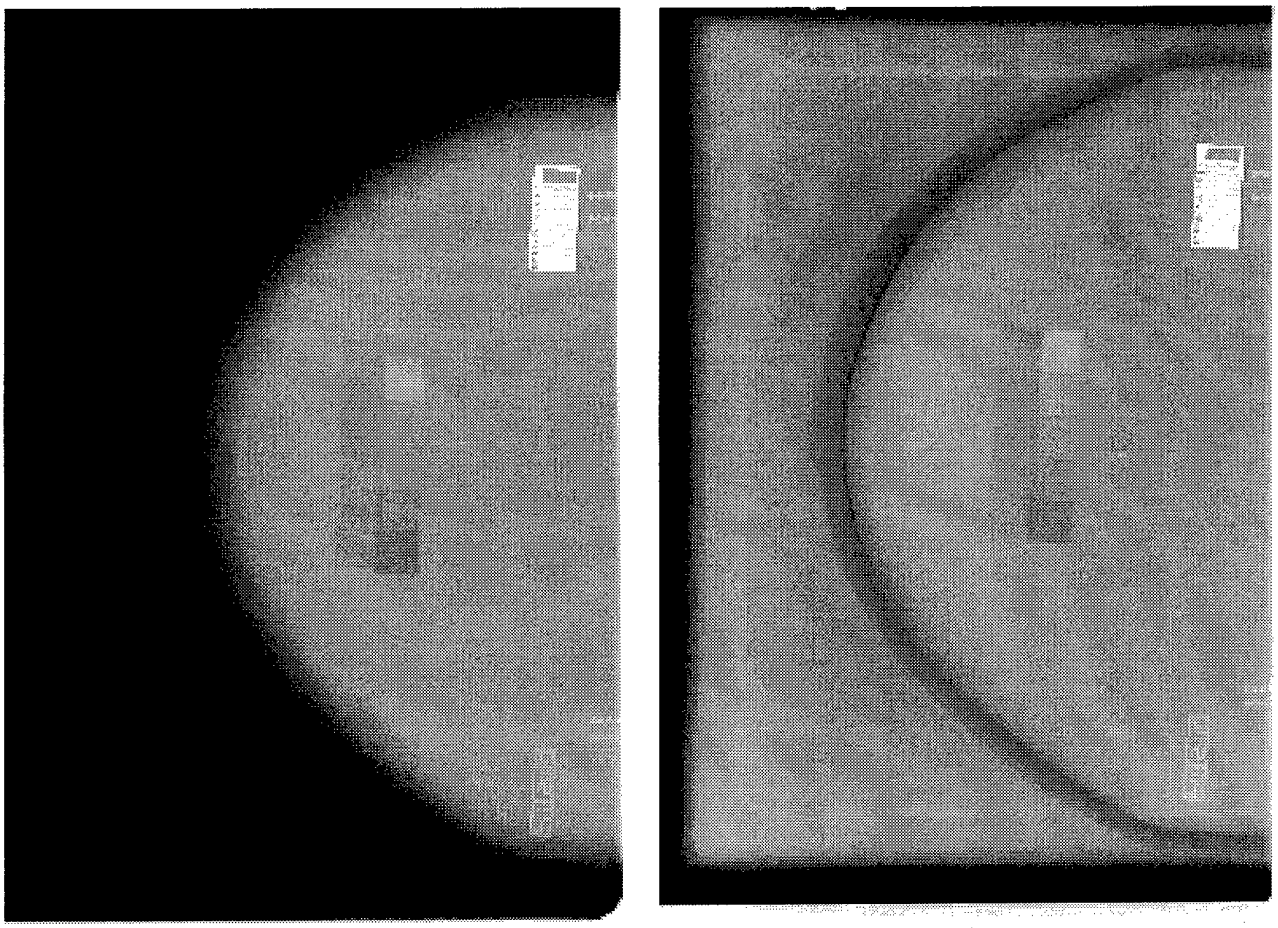

(a) (b)

Fig. 11. Comparison of (a) unequalized image and (b) equalized image of a CIRS phantom (4.5 cm thick 50% glandular/50% fat) exposed with a Mo/Mo 26 kVp beam. The phantom was immersed in a tissue-equivalent solution of alcohol and water in a container. The liquid was filled to the same thickness as the phantom.

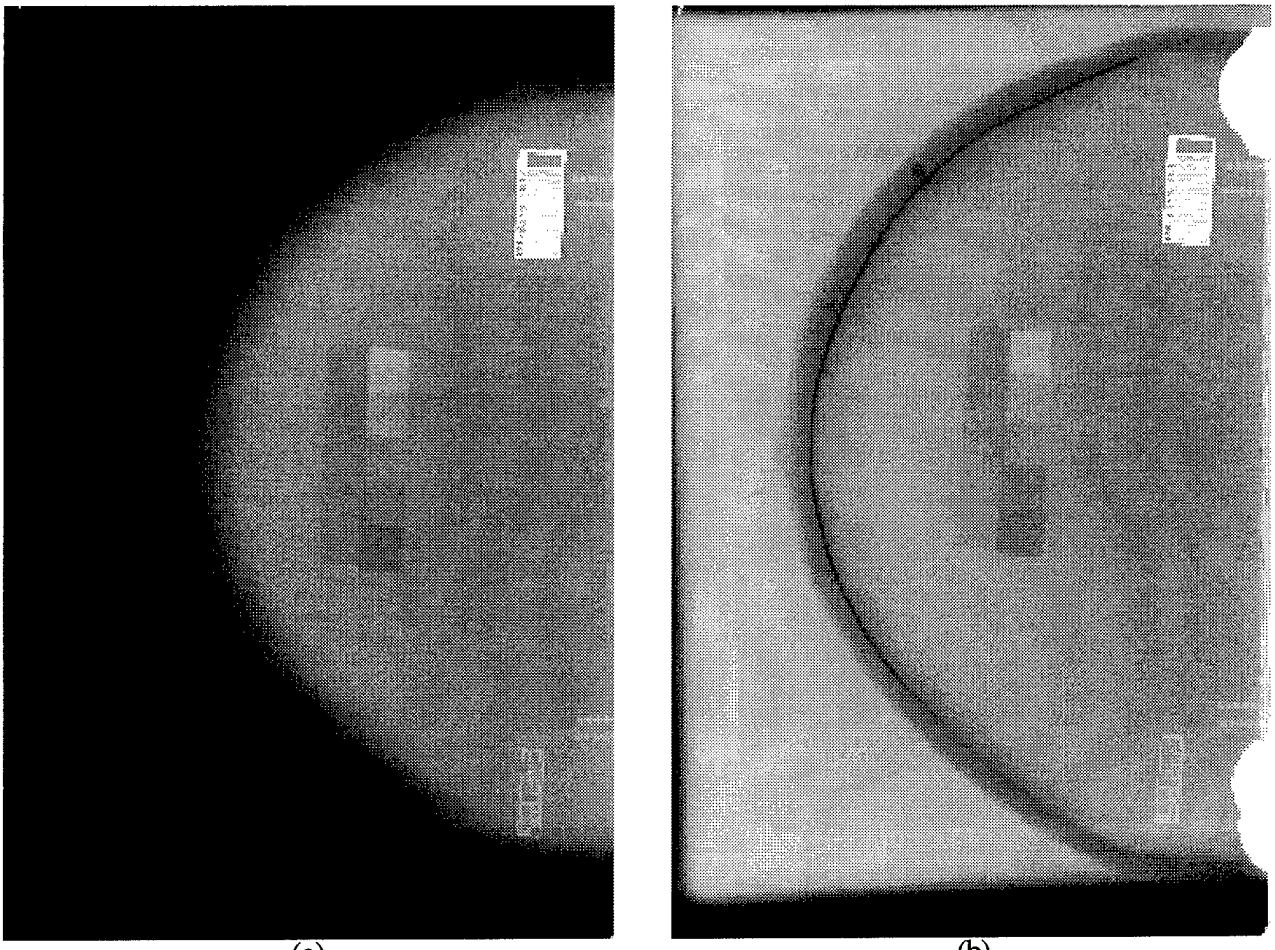

(a) (b)

Fig. 12. Comparison of (a) unequalized image and (b) equalized image of a CIRS phantom (4.5 cm thick 50% glandular/50% fat) exposed with a Mo/Mo 26 kVp beam. The phantom was immersed in a 50% fatty liquid in a container. The liquid was filled to the same thickness as the phantom.

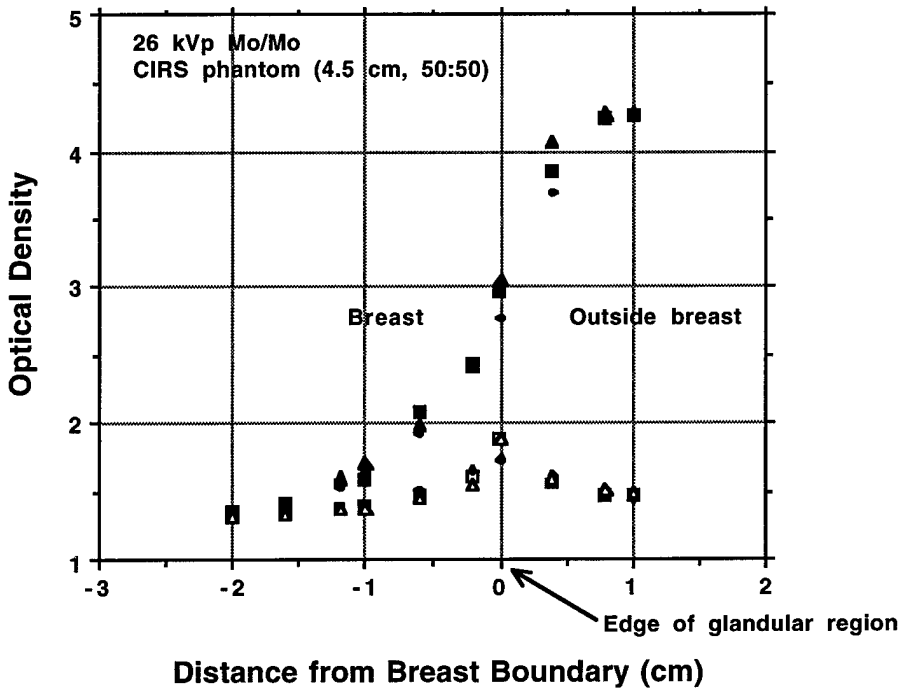

Fig. 13. Comparison of the optical density profiles of the unequalized and the equalized phantom images shown in Fig. 11. The optical densities were measured along three radii at the periphery of the phantom. The optical density profiles of the equalized image are much more uniform than those of the unequalized image. The low peak at about 0 cm corresponds with the fatty skin layer located at the periphery of the phantom.

(7) Conclusion

We have performed the following studies in the third year of the funding period: (1) completed the study of breast shape classification, (2) conducted a simulation study to evaluate the effects of x-ray equalization, (3) completed the Monte Carlo modeling of a mammographic imaging system with a focused antiscatter grid, (4) constructed prototype filters and evaluated filter alignment by imaging breast phantoms, (5) conceived an improved method for implementation of the x-ray equalization technique for mammography, (6) conducted preliminary studies to demonstrate the feasibility of the new approach, and (7) developed design specifications for the compressible tank component of the patient-specific and tissue-equivalent x-ray equalization system. The development of the new method is a significant step towards the practical implementation of the x-ray equalization technique.

(8) References

1. Shapiro S, Venet W, Strax P, Venet L, Roeser R: Ten-to-fourteen-year effect of screening on breast cancer mortality. JNCI 69:349-355, 1982.
2. Lester RG: The contributions of radiology to the diagnosis, management, and cure of breast cancer. Radiology 151:1-7, 1984.
3. American Cancer Society: Mammography guidelines 1983: Background statements and update of cancer-related checkup guidelines for breast cancer detection in asymptomatic women age 40 to 49. CA Cancer J Clin 33:255, 1983.
4. Moskowitz M: Breast cancer: Age-specific growth rates and screening strategies. Radiology 161:37-41, 1986.
5. Verbeek ALM, Hendriks JHCL, Holland R, Mravunac M, Sturmans F, Day NE: Reduction of breast cancer mortality through mass screening with modern mammography: First results of the Nijmegen project, 1971-1981, Lancet i:1222-1226, 1984.
6. Moskowitz M: Benefit and Risk. In: Breast Cancer Detection: Mammography and Other Methods in Breast Imaging. 2nd edition. Eds. Bassett LW, Gold RH. Grune and Stratton, NY, 1987.
7. Baker LH: Breast Cancer Detection Demonstration Project: A Five-Year Summary Report. CA Cancer J Clin 32:194-225, 1982.
8. American Cancer Society: Cancer Facts & Figures - 1987. Breast Cancer, p.10, 1987.
9. Baines CJ, Miller AB, Wall C, et al: Sensitivity and specificity of first screen mammography in the Canadian National Breast Screening Study: A preliminary report from five centers. Radiology 160:295-298, 1986.
10. Pollei SR, Mettler FA, Bartow SA, Moradian G, Moskowitz M: Occult breast cancer: Prevalence and radiographic detectability. Radiology 163:459-462, 1987.
11. Haug PJ, Tocino IM, Clayton PD, Bain TL: Automated management of screening and diagnostic mammography. Radiology 164:747-752, 1987.
12. D'Agincourt L: Technique is everything when breast is dense. Diagnostic Imaging, September: 57-61, 1993.
13. Wallis MG, Walsh MT, Lee JR: A review of false negative mammography in a symptomatic population. Clinical Radiology 44: 13-15, 1991.
14. Sickles EA: Mammographic features of "early" breast cancer. AJR 143:461-464, 1984.
15. Sickles EA: Mammographic features of 300 consecutive nonpalpable breast cancers. AJR 146:661-663, 1986.
16. Logan WW, Janus JA: Screen/film mammography. In: Breast Cancer Detection: Mammography and Other Methods in Breast Imaging. 2nd edition. Eds. Bassett LW, Gold RH. Grune & Stratton, NY, 1987.
17. Nishikawa RM, Mawdsley GE, Fenster A, Yaffe MJ: Scanned-projection digital mammography. Med Phys 14:717-727, 1987.
18. Nishikawa RM, Yaffe MJ: An investigation of digital mammographic imaging. Proc SPIE 419:192-200, 1983.

19. Bunch PC, Huff KE, Van Metter R: Analysis of the detective quantum efficiency of a radiographic screen/film system. J Opt Soc Am A 4:902-909, 1987.
20. Blackwell HR: Contrast thresholds of the human eye. J Opt Soc Am 36:624-643, 1946.
21. Baxter B, Ravindra H, Normann RA: Changes in lesion detectability caused by light adaptation in retinal photo-receptors. Invest Radiol 17:394-401, 1982.
22. Snyder HL: Chapter 3: The Visual System: Capabilities and Limitations. In: *Flat-Panel Display and CRTs*. Ed. Tannas LE Jr, Van Nostrand Reinhold, New York, 1985.

(9) Appendix

Publications in current year as a result of this grant

1. Goodsitt MM, Chan HP, Liu B. Investigation of the line-pair pattern method for evaluating mammographic focal spot performance. Medical Physics 1997; 24: 11-15.

2. Goodsitt MM, Chan HP, Liu B, Morton AR, Guru SV, Keshavmurthy S, Petrick N. Classification of compressed breast shape for the design of equalization filters in mammography. Submitted for publication in Medical Physics .

3. Keshavmurthy SP, Chan HP, Goodsitt MM. Design of exposure equalization filters for mammography. Presented at the 39th Annual Meeting of the American Association of Physicists in Medicine. Milwaukee, Wisconsin, July 27-31, 1997. Medical Physics 1997; 24: 1018.

4. Keshavmurthy SP, Chan HP, Goodsitt MM. Evaluation of x-ray detectors for digital mammography - Monte Carlo simulation study. Accepted for presentation at the 83rd Scientific Assembly and Annual Meeting of the Radiological Society of North America, Nov 30-Dec 5, 1997, Chicago, Illinois.